

Understanding the spatial interaction of ultrasounds based on three-dimensional dual-frequency ultrasonic field numerical simulation

Zhao-yang Yin¹, *Qi-chi Le¹, Yan-chao Jiang¹, Da-zhi Zhao², Qi-yu Liao², and Qi Zou¹

1. Key Lab of Electromagnetic Processing of Materials, Ministry of Education, Northeastern University, Shenyang 110819, China

2. School of Materials Science and Engineering, Northeastern University, Shenyang 110819, China

Copyright © 2024 Foundry Journal Agency

Abstract: A transient 3D model was established to investigate the effect of spatial interaction of ultrasounds on the dual-frequency ultrasonic field in magnesium alloy melt. The effects of insertion depth and tip shape of the ultrasonic rods, input pressures and their ratio on the acoustic field distribution were discussed in detail. Additionally, the spacing, angle, and insertion depth of two ultrasonic rods significantly affect the interaction between distinct ultrasounds. As a result, various acoustic pressure distributions and cavitation regions are obtained. The spherical rods mitigate the longitudinal and transversal attenuation of acoustic pressure and expand the cavitation volume by 53.7% and 31.7%, respectively, compared to the plate and conical rods. Increasing the input pressure will enlarge the cavitation region but has no effect on the acoustic pressure distribution pattern. The acoustic pressure ratio significantly affects the pressure distribution and the cavitation region, and the best cavitation effect is obtained at the ratio of 2:1 ($P_{15}:P_{20}$).

Keywords: dual-frequency ultrasonic; numerical model; acoustic pressure; spatial interaction; magnesium alloy

CLC numbers: TG146.22

Document code: A

Article ID: 1672-6421(2024)01-029-15

1 Introduction

Ultrasonics have the potential to alter physical, chemical, and biological properties of materials, making them highly promising for usage in engineering, earth science, and life science [1-3]. The widespread interest in ultrasonics originates from the various nonlinear effects it induces, including acoustic distortion, acoustic radiation pressure, cavitation effect, and acoustic streaming [4]. These nonlinear effects of ultrasonics offer a wide range of advantages including thermal effects, melt agitation, diffusion enhancement, and promotion of chemical reactions in the acting medium [5-7]. Nevertheless, the development of ultrasonic applications varies across different domains. Ultrasonic technology has found mature applications in surface cleaning, emulsification, dispersion, metal welding, and non-destructive testing. However, there are still several areas that require further improvement in the field of ultrasonics. These include

machining processes, extraction techniques, and metal melt treatment methods [8]. Among these areas, the ultrasonic treatment of molten metals holds significant prominence, and has been garnering increasing attention and development.

The research on ultrasonic treatment of metal melts began in the former Soviet Union. Sokolov's study showed that ultrasonic can refine the dendrites of various light metals and accelerate the solidification process [9]. In the following decades, ultrasound research entered a period of vigorous development. Researchers represented by Eskin et al. have carried out a number of experimental studies on power ultrasonic treatment of light alloys, especially aluminum alloy melts, showing that ultrasonic assisted direct-chill casting of aluminum alloys can achieve significant melt degassing and grain refinement effects [10-12]. The theory of ultrasonic degassing is applied to aluminum melts based on hydrogen measurements in as-cast alloys. The analytical model is found on the principal theory of bubble expansion and flotation caused by rectification diffusion of dissolved gases into oscillating bubbles. Another major application of ultrasonic is in the refinement of solidification structures. The explanation for the mechanism of ultrasound-induced refinement is not singular. The cavitation bubble absorbs heat from the

*Qi-chi Le

Ph. D, Professor. His research interests mainly focus on casting and solidification, plastic deformation of magnesium alloys, and development of new wrought magnesium alloys. To date, he has published more than 360 peer-reviewed papers and has been granted more than 70 patents.

E-mail: qichil@mail.neu.edu.cn

Received: 2023-04-02; Accepted: 2023-05-30

melt during formation and growth, creating local subcooling^[13]. At the moment of bubble collapse, the released high temperature, high pressure and micro jets will change the phase equilibrium and melting point of the local melt, thus increasing the nucleation rate. Studies on ultrasonic water modelling have demonstrated that cavitation bubbles can indeed alter local phase equilibrium and melting point and cause local subcooling that favors nucleation. Ultrasound-induced undercooling has also been observed in low melting point metals such as Bi and Bi-Sn alloys^[14]. It is believed that the cavitation effect will break the primary nuclei and dendrites to inhibit the growth of dendrites, while the acoustic flow effect will promote the dispersion of tiny nuclei. These two effects work together to achieve the solidification refinement effect^[15]. Moreover, it has also been suggested that ultrasonic treatment could increase the wettability of inclusions (oxides) in the molten metal, resulting in acoustic-induced capillary effect and thus promote heterogeneous nucleation^[16-17]. Unfortunately, due to the opacity and high temperature of the molten metal, there is no direct evidence for the above conjecture. Although the mechanism of ultrasonic melt treatment is not very clear, the effect of ultrasonic on improving the solidification structure of metal is beyond doubt, which has been proven by a great number of research results. Both technological practice and theoretical research show that ultrasonic treatment of metal melt has better microstructure refinement effect than electromagnetic treatment.

Although ultrasonic melt treatment has shown unique advantages and broad prospects, the industrial application of this technology still faces many difficulties. These difficulties include the strong attenuation of acoustic energy in the melt and the instability of the physical parameters of the melt during production. In recent years, some adverse factors restricting the application of ultrasound have been gradually overcome. For example, the maximum power of high intensity ultrasonic transducers is up to 5 kW. However, problems, such as the severe attenuation of ultrasound in molten metals, which are inherent to the nature of ultrasound, are obstacles to the application of ultrasonic in melt processing. Studies have shown that variable frequency (real-time frequency variation) and multiple frequency (combination of different frequencies) ultrasound modalities are effective in enhancing the non-linear effects of ultrasound compared to conventional single-frequency ultrasonic field^[18-19]. Multi-frequency ultrasonic has been applied in the fields of sonochemistry, fluid engineering and medical diagnostics. Studies in fields such as acoustic catalysis and sonochemistry have shown that multi-frequency resonance can enhance cavitation efficiency and optimize the effect of ultrasonic treatment. Feng et al.^[20] found that 28 kHz+0.87 MHz dual-frequency resonance and 28 kHz+1 MHz+1.87 MHz triple frequency resonance significantly increased the cavitation yield, and suggested that multi-frequency resonance could significantly enhance the perturbation effect of ultrasonic on the sample solution and may even disrupt the surface continuity of the solution, thus increasing the number of cavitation nuclei. Brotchie et al.^[21] found that acoustic luminescence and sonochemical reactions

were significantly enhanced under dual-frequency excitation at 20 kHz+355 kHz. Qin et al.^[22] found in the experiment on rice degradation by ultrasonic that dual-frequency ultrasonic not only improved the degradation efficiency but also increased the extraction rate of cadmium compared to single-frequency ultrasonic, and the frequency selection of dual-frequency ultrasonic field was also a crucial factor.

Dual-frequency ultrasonic has been applied to magnesium alloy melt treatment on the basis of its good response in various fields^[23]. Results show that variable frequency ultrasonic and dual-frequency ultrasonic are more effective in refining the as-cast structure and improving the morphology and distribution of the second phase at the same power compared to single-frequency ultrasonic. For example, the grain refinement efficiency of ZK60 magnesium alloy subjected to dual-frequency ultrasonic was 30.1% higher than single-frequency ultrasonic, and the yield strength, tensile strength and elongation of ingots were increased by 20.5%, 20.7%, and 30.0%, respectively^[23]. Dual-frequency ultrasonic not only overcomes the severe attenuation of acoustic energy to a greater extent, but also solves the complex electrical control system problem of variable frequency ultrasonic, showing greater application potential. As a new melt processing technology, its application method and effect need to be further improved and optimized, which depends on the in-depth research on its essential mechanism. Various influence factors are to be studied for dual-frequency ultrasonic, such as the frequencies combination, the choice of input pressure, the spatial position of the radiating rods, the design of the rod shape, etc. Few literature reports were found to discuss the influence of dual-frequency ultrasonic and its characteristic parameters on metal preparation.

Therefore, to investigate the impact of spatial interaction of ultrasounds on dual-frequency ultrasonic treatment, a transient 3D model of pressure acoustics was developed. AZ80 magnesium alloy was selected as the experimental material. The influences of the spatial position and tip shape of ultrasonic rods, input pressures and their ratios on the distribution of acoustic pressure and corresponding cavitation area within the system were discussed in detail. The primary objective of this study is to provide fundamental data and process optimization for the preparation of magnesium alloy using dual-frequency ultrasonic technology. By uncovering the underlying mechanisms of this technology, it can lead to advancements in related equipment development and promote its industrial applications. Additionally, a deeper understanding of dual-frequency ultrasonics can facilitate research into new ultrasound processes, opening up possibilities for innovative applications in various fields.

2 Numerical methodology

2.1 Geometric model

Figure 1 shows the 3D geometric model in this numerical simulation. The AZ80 magnesium alloy melt to be processed in the crucible is regarded as a cylindrical model with a height of 350 mm and a radius of 100 mm. Two ultrasonic rods with a

diameter of 30 mm were introduced from above the liquid level and inserted into the melt at a certain depth. Point O is the center point of the top surface. Points A and B are situated on the top surface, with Point A being 35 mm away from Point O and Point B being 70 mm away from Point O. The Line AB is perpendicular to the longitudinal section of the model. Points M and N are positioned at the center points of the 15 kHz ultrasonic radiator and 20 kHz ultrasonic radiator, respectively. Points P and P₁ are located in the cross-section of z=300 mm, Point P₁ is at the top edge, and the Line PP₁ is perpendicular to the longitudinal section. Points O₁, A₁, B₁, M₁, and N₁ are projection points of Points O, A, B, M, and N at the bottom.

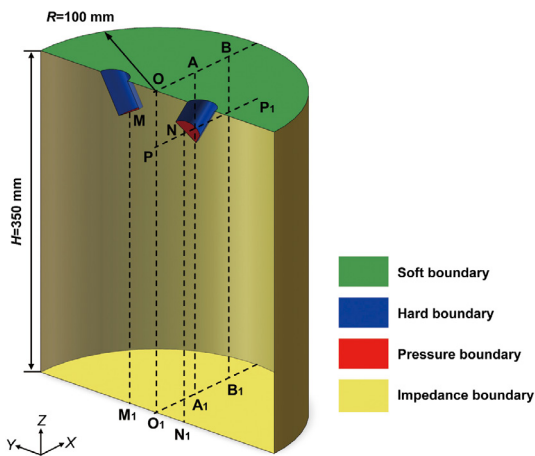


Fig. 1: Schematic diagram of a 3D geometric model for dual-frequency ultrasonic treatment

2.2 Meshwork

The accuracy of calculations is closely linked with the choice of mesh size. Table 1 lists the sizes and types of three different meshes shown in Figs. 2(a-c). To select a reasonable mesh size, the acoustic pressure distribution along Line OO₁ was calculated for several cases with different mesh sizes (mesh type: free tetrahedron), as shown in Fig. 2. It is evident that the calculation results in these three cases are nearly identical, indicating that all the three mesh size settings meet the requirements for accurate calculations. However, the smaller the maximum cell size, the larger the number of domain units generated, which significantly increases the computational effort and solution time. To balance the computational accuracy and solution time, the mesh with a maximum size of 10 mm is a more sensible choice.

Table 1: Size and type of mesh

Maximum unit size (mm)	Number of domain units
8	1,018,756
10	592,026
12	304,735

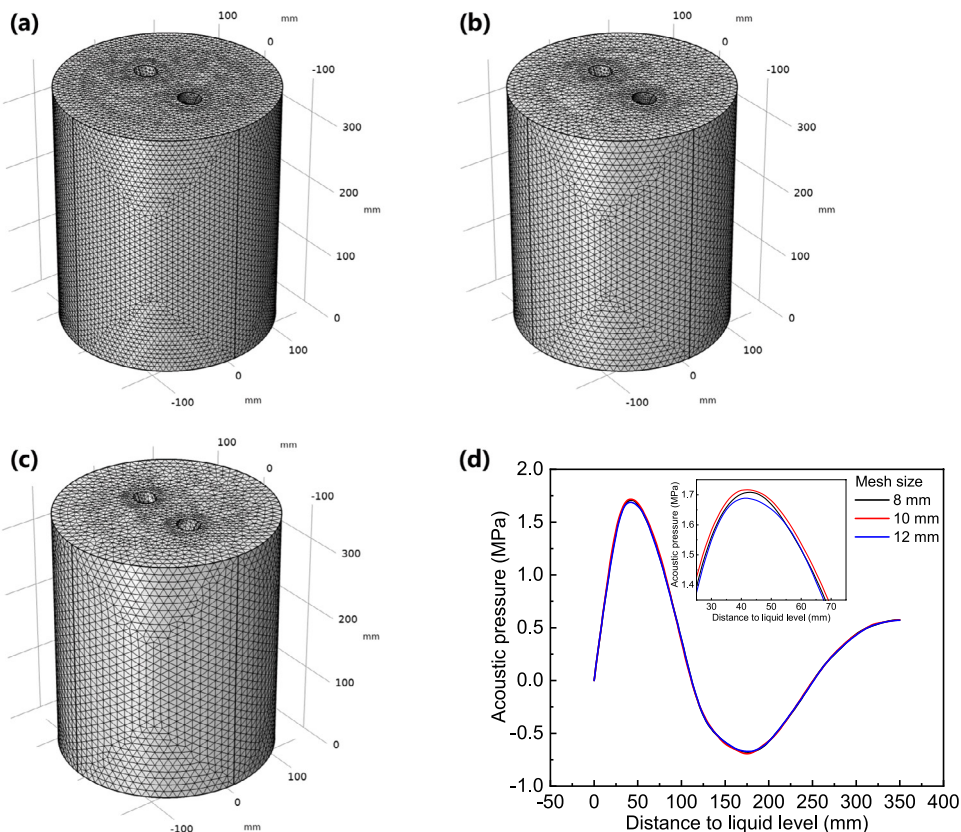


Fig. 2: Mesh for acoustic pressure distribution calculation with different maximum sizes of 8 mm (a), 10 mm (b), 12 mm (c), and calculated acoustic pressure distribution along Line OO₁ (d)

2.3 Governing equations

The equation used to describe sound waves in a melt is derived from the governing equation of fluid flow, which is expressed as [24]:

$$\frac{1}{\rho c^2} \frac{\partial^2 p}{\partial t^2} - \nabla \left[\frac{4\mu}{3\rho} \nabla \left(\frac{1}{\rho c^2} \frac{\partial p}{\partial t} \right) \right] - \nabla \left(\frac{1}{\rho} \nabla p \right) = \frac{\partial}{\partial t} \left(\frac{Q}{\rho} \right) - \nabla \left[\frac{4\mu}{3\rho} \nabla \left(\frac{Q}{\rho} \right) \right] \quad (1)$$

where ρ is the average density of the melted medium, c is the acoustic velocity in the melt, p is the acoustic pressure, t is the time, μ is the dynamic viscosity of the melt, and Q is the mass source term in the continuity equation.

Since the dynamic viscosity of the alloy melt in the liquid phase is small, the mass source term Q can be ignored to simplify the acoustic field calculation. Assuming that the melt medium is incompressible, the melt flow is adiabatic and the ultrasonic maintains the property of linear propagation in the homogeneous melt medium, the Eq. (1) can be simplified as:

$$\frac{1}{\rho c^2} \frac{\partial^2 p}{\partial t^2} - \nabla \left(\frac{1}{\rho} \nabla p \right) = 0 \quad (2)$$

Assuming that the ultrasound remains resonant in the melt medium, the Eq. (2) can be solved by a finite method in the COMSOL Multiphysics analysis software, and a solution of the form is obtained as:

$$P(x, y, z, t) = p(x, y, z) e^{i\omega t} \quad (3)$$

where x , y and z are the space coordinates, ω is the angular frequency of the acoustic wave, given by $\omega=2\pi ft$ (f is the ultrasonic frequency), P is transient acoustic pressure, e is natural constant, and i represents the imaginary number. Then, the spatial variation of the acoustic pressure $p(x, y, z)$ can be given by solution of the Helmholtz equation [25]:

$$\nabla \left(\frac{1}{\rho} \nabla p \right) - \frac{\omega^2}{\rho c^2} p = 0 \quad (4)$$

The propagation behavior of ultrasonic waves in a melt can be calculated by the Helmholtz equation [Eq. (4)] as long as the acoustic pressure boundary conditions of the physical model and the vibration frequency and propagation velocity of the ultrasonic waves in the melt are determined. It should be noted that to obtain an accurate numerical solution of the Helmholtz equation, the discretization step size h should be adjusted to satisfy the following condition:

Table 2: Parameters used in this simulation

Parameters (unit)	Description	Value
f (kHz)	Frequency of ultrasound	15, 20
p_0 (MPa)	Total input acoustic pressure	5.4 (2.7+2.7)
ρ (kg·m ⁻³)	Density of melt	1,780
c (m·s ⁻¹)	Speed of ultrasound in melt	4,000
μ (Pa·s)	Dynamic viscosity of melt	1.12×10 ⁻³
P_B (MPa)	Cavitation threshold	0.9
Z (Pa·s·m ⁻¹)	Impedance	4.1×10 ⁷

$$\frac{h}{\lambda} \ll 1 \text{ or } k \cdot h = \text{constant} \quad (5)$$

where λ is the wavelength and k is the wave number ($k=\omega/c$). However, under this condition, the errors of the finite element solution increase sharply as the wave number k increases, which is termed as pollution effect. To overcome this problem, an adequate refined mesh was used, which was clarified in Subsection 2.2.

2.4 Boundary conditions

Figure 1 illustrates the four boundary conditions defined in this geometric model: (1) the end surfaces of the ultrasonic rods are defined as the pressure boundaries, $p=p_0 \sin(2\pi ft)$, where p_0 is the initial acoustic pressure; (2) the interface between the melt and air is defined as a soft boundary, where $p=0$; (3) the side walls of the ultrasonic rods inserted into the melt are defined as the hard boundaries, where $\partial p/\partial n=0$; (4) the inner wall of the crucible is defined as the impedance boundary, $(1/p(\partial p/\partial n))+(i\omega t/Z)=0$, where Z is the acoustic input impedance of the external domain, n refers to the outer normal direction of domain boundary. The acoustic parameters and the physical properties of the AZ80 magnesium alloy required in this numerical simulation are described in Table 2.

In the negative pressure phase of the acoustic field, the initial cavitation nuclei in the liquid grow into cavitation bubbles as a result of tensile stress, and then they expand or even collapse. Therefore, the minimum acoustic pressure required to generate the cavitation effect is defined as the cavitation threshold P_B . Based on the assumption of "cavitation nucleus", the cavitation threshold is closely related to the equilibrium radius R_0 of the cavitation nucleus according to the analysis and calculation of the stability of the initial cavitation nucleus in liquids. A larger equilibrium radius (R_0) corresponds to a smaller cavitation threshold, which increases the possibility of generating cavitation effects. According to our previous work, the cavitation threshold for AZ80 magnesium alloy in this simulation model was set to 0.9 MPa [26]. The value of the impedance Z can be calculated from the equation $Z=\rho_i c_i$ [27], where ρ_i and c_i are the density and speed of sound of the impedance boundary (inner wall of the crucible), respectively. In this model, the impedance Z is calculated to be $4.1 \times 10^7 \text{ Pa}\cdot\text{s}\cdot\text{m}^{-1}$.

2.5 Convergence study

The physical field interface of this numerical model was transient pressure acoustics. The maximum number of nonlinear iterations of the

calculation process was set to 4, the termination technique of model calculation was Tolerance, and the Tolerance factor was set to 1. To ensure that the calculation time is sufficient to judge the stability of the calculation results, the output time was set to $30 \times T_{20}$ in this model, where T_{20} is a cycle of the ultrasonic frequency of 20 kHz. Considering the accuracy of the calculation results and the calculated amount, the calculation step was set to $T_{20}/15$, as further reduction of the step size cannot improve the accuracy of the calculation. Figure 3 shows the variation of the acoustic pressure at the midpoint of the Line OO_1 under the dual-frequency ultrasonic treatment. The acoustic pressure shows a regular variation within the set computation time. In other words, the calculation results under this parameter setting are stable, i.e., the convergence of the model is guaranteed.

3 Results and discussion

3.1 Effect of rod spacing on dual-frequency ultrasonic melt treatment

The numerical calculation of the ultrasonic fields with different spacings of ultrasonic rods was carried out to explore the effect of the rod spacing on the dual-frequency ultrasonic melt treatment. The insertion depth and included angle of two ultrasonic rods are set to 30 mm and 60° . Five different rod spacings were selected, ranging from 30 mm to 150 mm. The tip shape of radiating rod is flat unless otherwise stated. Figure 4 shows the acoustic pressure distributions in the melt with different rod spacings. The highest acoustic pressure region is always concentrated at the radiating surface, and the acoustic pressure attenuates rapidly as the ultrasonic wave propagates in the melt. Ultrasonic-induced cavitation is the key to grain refinement of ultrasonic melt treatment [5, 28]. Cavitation events can be triggered when the acoustic pressure inside the melt is

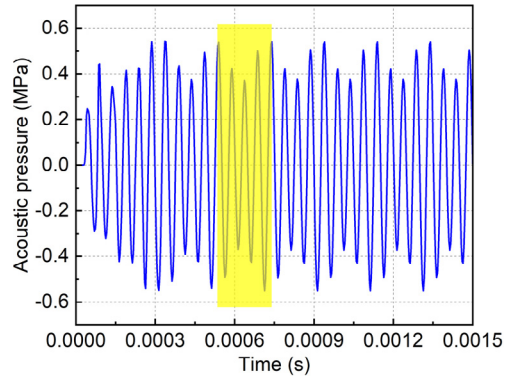


Fig. 3: Verification of convergence of numerical model

greater than the melt cavitation threshold. The specific derivation process is not demonstrated in this study. The corresponding cavitation regions calculated for different rod spacings are displayed on the left side of the figure in a mirrored fashion. With a rod spacing of 30 mm, the high acoustic pressure area is in the ellipsoid shape near the ultrasonic rods, as shown in Fig. 4(a). In the cases of 60 mm and 90 mm, the cavitation regions are elongated into a peanut shape, as shown in Figs. 4(b, c). When the rod spacing is further increased to 120 mm or 150 mm, the cavitation region in the melt only appears at the radiating surface of the two rods, as shown in Figs. 4(d, e). Figure 4(f) illustrates the cavitation volume at different rod spacings. The cavitation volume tends to increase and then decrease with the increase of the rod spacing. The maximum cavitation area can be obtained at the rod spacing of 60 mm.

The greatest contributor to grain refinement by ultrasound is acoustic cavitation [29]. The ultrasonic parameters are crucial for the intensity of acoustic cavitation [30-31]. In our previous work, characteristic parameters such as ultrasound frequency and power have a significant effect on acoustic pressure, cavitation range and thus change the treatment effect. In this study, the

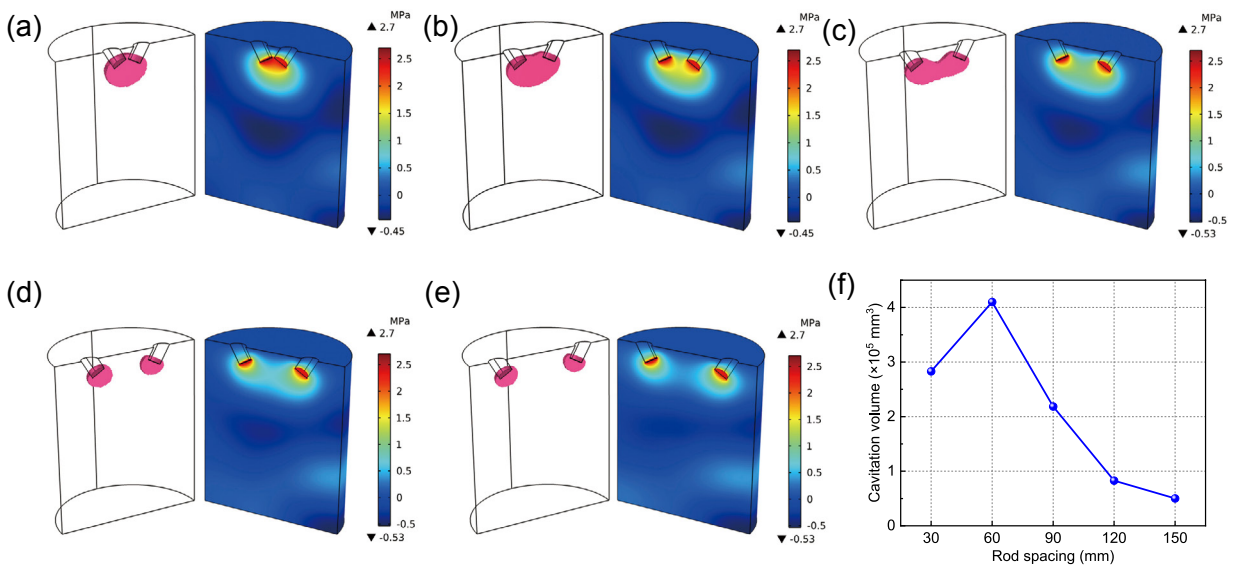


Fig. 4: Acoustic pressure distributions and corresponding cavitation regions of dual-frequency ultrasonic with different rod spacings: (a) 30 mm; (b) 60 mm; (c) 90 mm; (d) 120 mm; (e) 150 mm; (f) statistical results of cavitation volume

larger cavitation zone of the dual-frequency ultrasound field obtained under different conditions corresponds to a higher cavitation efficiency. Obviously, for ultrasound-assisted casting of magnesium alloy, the larger the cavitation range, the more cavitation bubbles can be excited and the greater the degree of grain refinement can be obtained. To better understand the effect of rod spacing on the acoustic pressure field, a comparative analysis of the acoustic pressure distribution along different sectional lines was carried out, and the results are shown in Fig. 5. The gray dashed line represents the melt cavitation threshold. As seen from Figs. 5(a, b), at the position near the radiating surface, the larger the rod spacing, the more drastic the acoustic pressure attenuation, and thus the smaller the excited cavitation region. The acoustic pressure at a depth of 75 mm decreases from 2.7 MPa at the radiating surface of the 15 kHz rod to 1.05 MPa–0.43 MPa, respectively. The acoustic pressure decreases to 1.07 MPa–0.27 MPa from the surface of the 20 kHz rod. The attenuation degree of acoustic pressure at different rod spacings corresponds to the volume of the cavitation. For example, at small rod spacings (e.g. 30 mm, 60 mm), the acoustic pressure attenuates slowly and a large cavitation volume is obtained. Conversely, the acoustic pressure attenuates quickly at large spacings (e.g. 120 mm, 150 mm), giving a small cavitation volume, as shown in Fig. 4(f). Not much consideration is given to the acoustic pressure distributions further away from the ultrasonic rods due to the absence of cavitation behavior. A similar regularity is obtained by calculating the acoustic pressure at different distances from the center of the melt. As shown in Figs. 5(c, d), the acoustic

pressure amplitudes along both AA₁ and BB₁ decrease with the increase of rod spacing.

The above simulation results indicate that increasing the rod spacing will not only aggravate the attenuation of the longitudinal acoustic pressure in the melt but also lead to the decrease of the transverse acoustic pressure. In other words, the interaction of ultrasound is significantly influenced by the rod spacing. Large rod spacing weakens the interaction enhancement between two ultrasounds, leading to a decrease in the cavitation effect. However, the optimum cavitation effect is not obtained at the minimum rod spacing. This is because, at a small rod spacing, the area where the interaction of the two ultrasounds occurs is small and the acoustic pressure decays rapidly. Therefore, a moderate rod spacing is an important factor to obtain an excellent cavitation effect for dual-frequency ultrasonic.

3.2 Effect of rod angle on propagation and interaction of acoustic waves

The effect of the included angle of ultrasonic rods, ranging from 0° to 120°, on the distribution of acoustic pressure was investigated. The spacing between the rods was set at 60 mm, and the insertion depth was set at 30 mm. Figures 6(a–e) presents the acoustic pressure distribution and the corresponding cavitation region at different included angles. When both rods are inserted vertically into the melt, the acoustic interaction is stronger in the radial direction than in the longitudinal direction, and an ellipsoidal-like high acoustic pressure region is obtained, as shown in Fig. 6(a). By inserting the two ultrasonic rods at a

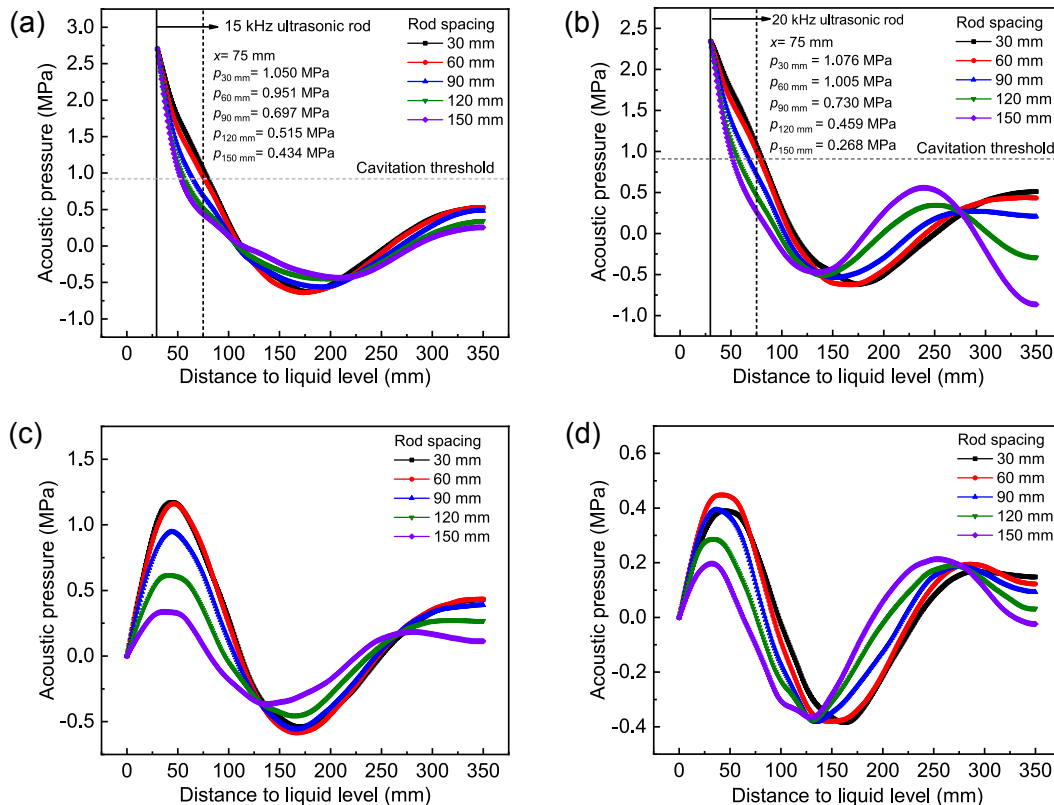


Fig. 5: Acoustic pressure distribution of dual-frequency ultrasonic treatment along Lines MM, (a), NN, (b), AA₁ (c) and BB₁ (d)

certain angle of toward the melt center, the radial acoustic pressure decays more rapidly than the longitudinal one, so that the high acoustic pressure region in the melt tends to be more spherical. Figure 6(f) shows the 2D cavitation area and cavitation volume of the YZ section for different ultrasonic rod angles. At small angles of 0–60°, the cavitation volume tends to increase slightly with the increase of the included angle, with a volume of about $4.1 \times 10^5 \text{ mm}^3$. When the angle increases to 90° and 120°, the cavitation volume significantly decreases to about $3.7 \times 10^5 \text{ mm}^3$. Accordingly, to optimize the cavitation effect of dual-frequency ultrasonic, it is necessary to choose the proper ultrasound rod angle. An excessive included angle of the ultrasonic rods will weaken the cavitation strength, and an included angle of 60° is a wise choice to obtain a larger cavitation volume.

3.3 Effect of rod insertion depth on acoustic pressure distribution

Figure 7 shows the acoustic pressure distributions in the melt with different rod insertion depths from 10 mm to 110 mm, with a rod spacing of 60 mm and an included angle of 60°. As the insertion depth increases, the high acoustic pressure region shifts from the upper half of the melt to the center, and the size and shape of the potential cavitation region change considerably. When the ultrasonic rod is inserted at a depth of 10 mm, the high acoustic pressure area only appears below the liquid level and diminishes rapidly. The acoustic pressure at the center and bottom of the melt is relatively low. When the insertion depth reaches 30 mm and 50 mm, the acoustic pressure at the waist and bottom of the melt increases and the effective cavitation area is significantly expanded. Interestingly, no expansion but a slight decrease in the cavitation area is observed with further increasing the insertion depth. The cavitation area above the ultrasonic rods increases slightly, while the cavitation area below becomes smaller, as shown in Figs. 7(d–f). The acoustic pressure at the bottom of the melt increases, while the acoustic

pressure at the waist position gradually decreases. Additionally, the acoustic pressure at the bottom of the melt is increased as the ultrasonic rod is immersed deeper. Figure 7(g) shows the statistical results of cavitation volume with different insertion depths of ultrasonic rods. In the case of the insertion depth of 10 mm, the cavitation volume is only $0.84 \times 10^5 \text{ mm}^3$. In the case of 30 mm insertion depth, the cavitation volume increases dramatically to $4.1 \times 10^5 \text{ mm}^3$, with an expansion of several times. The effective cavitation range does not show a monotonic increase or decrease with the increase of insertion depth but reaches a maximum at an insertion depth of 50 mm.

The acoustic pressure distributions along MM_1 and NN_1 with different insertion depths were calculated to explore the reasons behind this phenomenon. As seen from Fig. 8, the ultrasonic wave is emitted from the surface of the acoustic rod and propagates in the melt, with the acoustic pressure showing a tendency to decay and then increase. To study the acoustic pressure attenuation at different insertion depths, the distance at which the acoustic pressure decays along MM_1 to 1.0 MPa with different insertion depths is marked in Fig. 8(a). The acoustic pressure in the case of 30 mm insertion depth attenuates to 1.0 MPa at the position that is 45 mm far from the radiating surface of the rod. The acoustic pressure attenuates to 1.0 MPa at a distance of 27 mm and 26 mm in the case of 90 mm and 110 mm insertion depth, respectively. The greater the insertion depth, the shorter the distance the acoustic pressure decays to 1.0 MPa. The same rule is obtained by calculating the acoustic pressure distribution along the NN_1 . A shorter distance means that the acoustic pressure decays faster in the melt. The sound intensity I in the melt is positively related to the acoustic pressure and decreases with the increase of the propagation distance, which is expressed as follows:

$$I = I_0 e^{-\alpha x} \quad (6)$$

where I_0 is the initial sound intensity, α is the attenuation coefficient, and x is the propagation distance. Due to the high

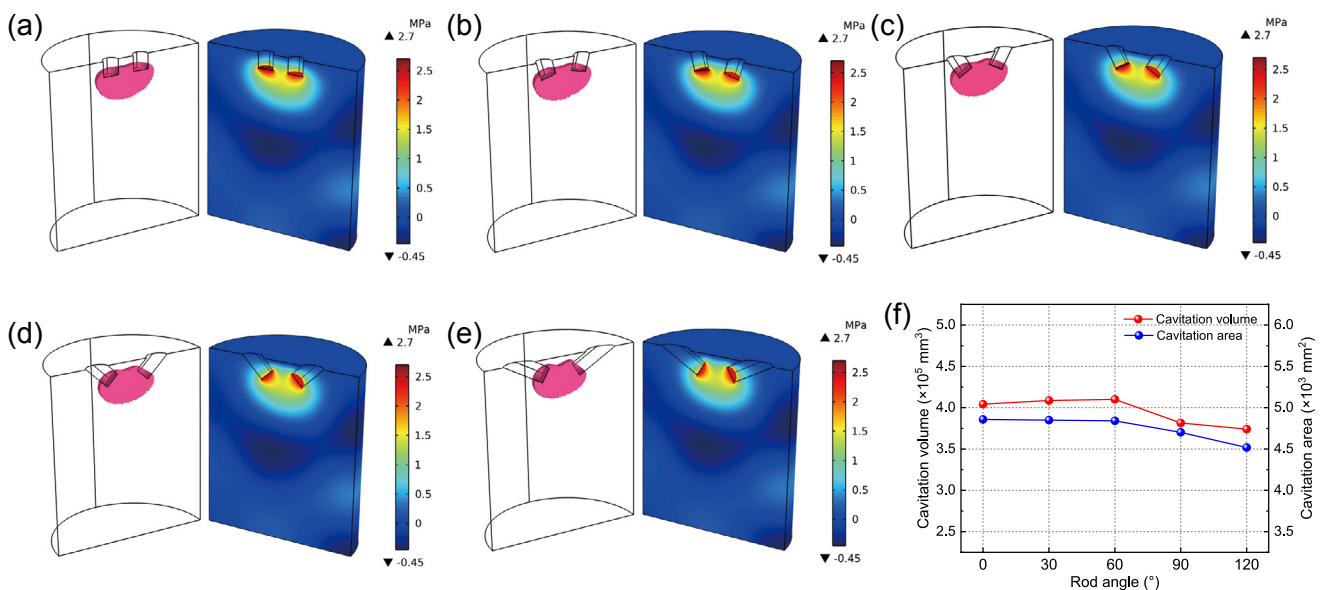


Fig. 6: Acoustic pressure distribution and corresponding cavitation area of dual-frequency ultrasonic treatment with different rod angles: (a) 0°; (b) 30°; (c) 60°; (d) 90°; (e) 120°; (f) statistical results of cavitation volume

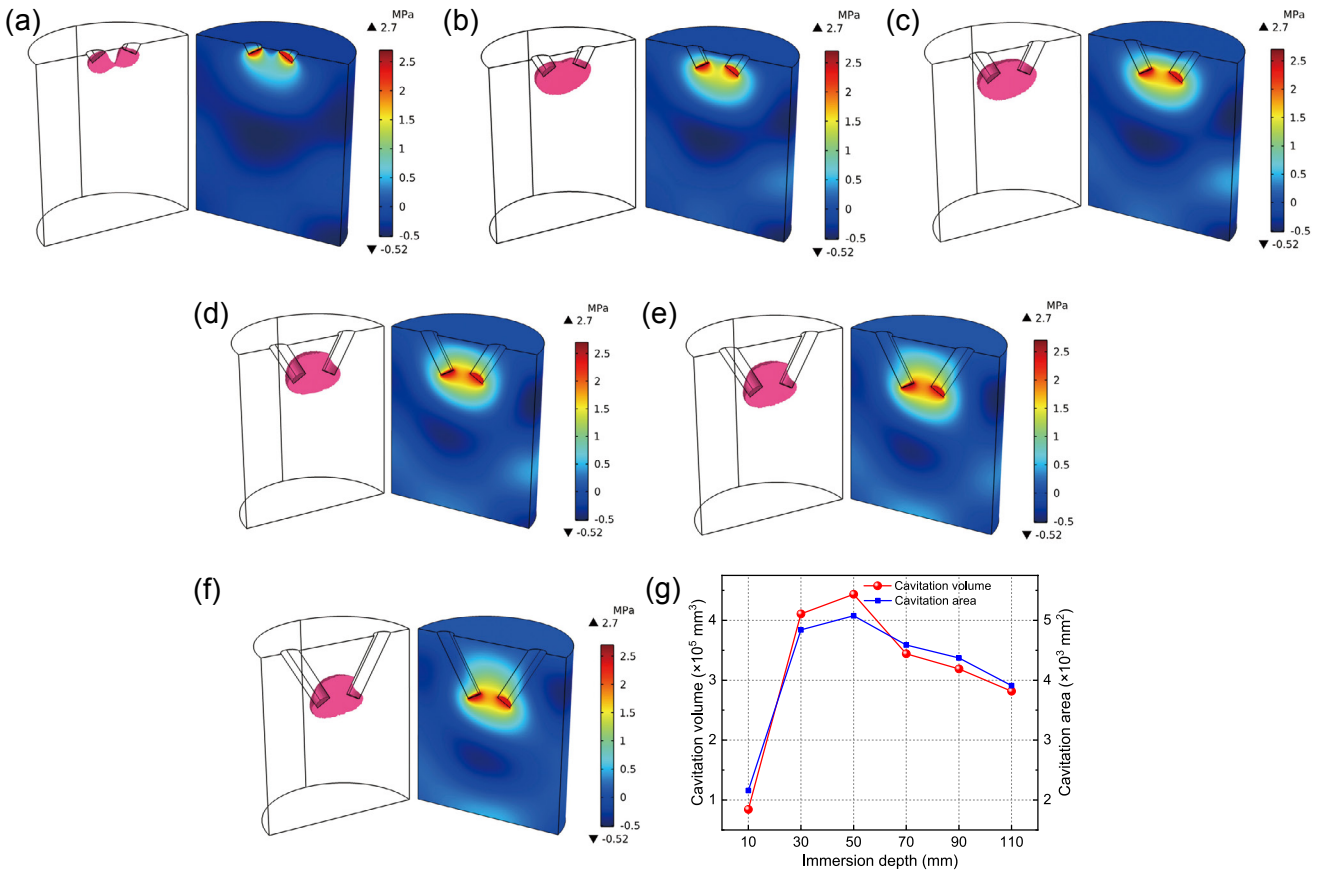


Fig. 7: Acoustic pressure distribution and corresponding cavitation volume of dual-frequency ultrasonic treatment with different immersion depths: (a) 10 mm; (b) 30 mm; (c) 50 mm; (d) 70 mm; (e) 90 mm; (f) 110 mm; (g) statistical results of cavitation volume

temperature and viscosity of the magnesium alloy melt, the energy of the ultrasonic waves will be attenuated as they propagate within the melt, causing a reduction in the acoustic pressure gradient [32]. The acoustic pressure exhibits different degrees of attenuation at different insertion depths of ultrasonic rods, as shown in Fig. 8. Minimal attenuation is observed at 30 mm insertion depth, but the largest cavitation volume is observed at 50 mm depth. Unfortunately, some related studies have shown that in single-frequency ultrasonic experiments, the greater the insertion depth of the ultrasonic rod, the larger the composition subcooling region will be formed, which will lead to severe macroscopic segregation in the central region of the melt and reduce the ingot quality [33]. Therefore, the ultrasound rod should not be immersed too deep.

In summary, the insertion depth of ultrasonic rods is one of the critical factors affecting the acoustic pressure distribution of dual-frequency ultrasonic. To obtain a higher efficiency of ultrasonic vibration, it is crucial to choose the appropriate insertion depth. In this model, an insertion depth of 30 mm is a wise choice.

3.4 Effect of rod tip shape on effect and efficiency of ultrasonic processing

The ultrasonic rod, in direct contact with the melt, is an essential component for radiating ultrasonic waves to the processing object. Ultrasonic waves are injected directly into the melt from the radiating surface of the ultrasonic rods, so the tip shape is critical

to transmitting ultrasonic energy. A reasonable design of the tip shape of the rods is the key to ensuring the effect and efficiency of ultrasonic processing. Therefore, three physical models of different tip shapes of the ultrasonic rod were established in this section to explore the effect of tip shapes on the acoustic field distribution of dual-frequency ultrasonic. The rod spacing, included angle, and insertion depth were set to 60 mm, 60°, and 30 mm, respectively. Figure 9 shows the acoustic pressure distribution and corresponding cavitation area for the case of a flat rod, a conical rod, and a spherical rod. In the case of a spherical rod, the high acoustic pressure area near the rod is enlarged, and the acoustic pressure at the waist and bottom of the melt is significantly improved compared with the flat rod. The effect of the conical rod is somewhere in between. The calculated cavitation volume for the three cases is shown in Fig. 9(d). The cavitation volume of the spherical rod is $6.3 \times 10^5 \text{ mm}^3$, which is 53.7% and 31.3% larger compared to flat and conical rods, respectively. The different scales of the cavitation area are caused by the difference in ultrasonic wave propagation within the melt. Figure 10 illustrates the acoustic pressure distributions for the $z=300 \text{ mm}$ cross-section. The acoustic pressure decays from 2.70 MPa to 1.65 MPa, 1.82 MPa and 1.96 MPa for the three conditions as the ultrasound propagates from the radiating surface of the rods. This indicates that a higher longitudinal acoustic pressure gradient is obtained within the melt in the case of the spherical rod. The acoustic pressure at different distances from the center of the melt was calculated, as shown

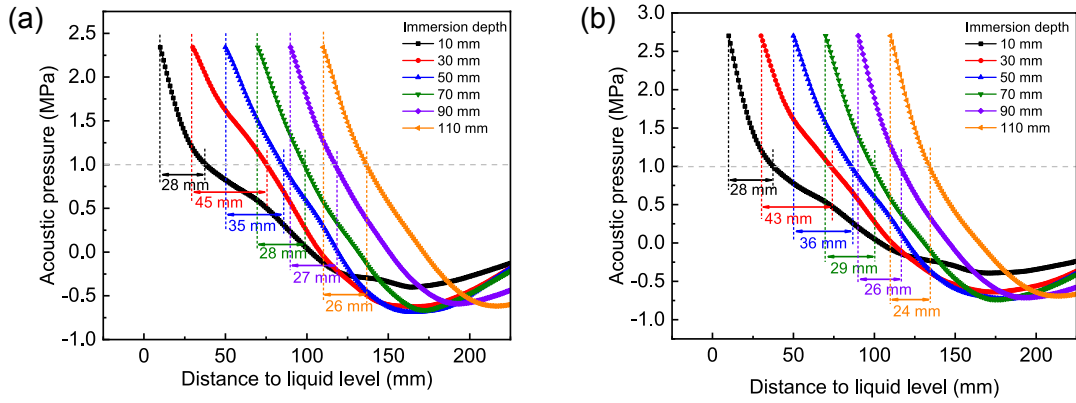


Fig. 8: Acoustic pressure distribution of dual-frequency ultrasonic treatment along MM₁ (a) and NN₁ (b)

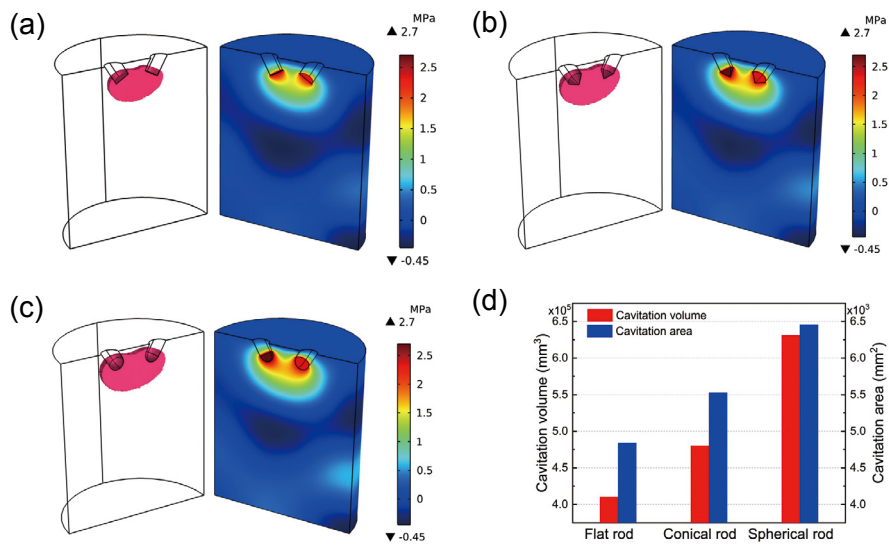


Fig. 9: Acoustic pressure distribution and corresponding cavitation volume of dual-frequency ultrasonic treatment with different tip shapes: (a) flat surface; (b) conical surface; (c) spherical surface; (d) statistical results of cavitation volume

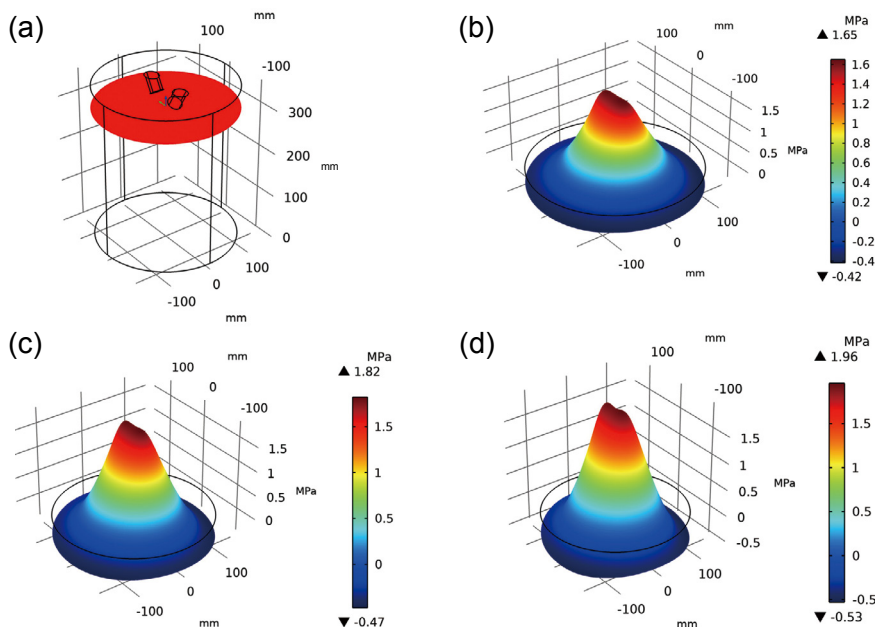


Fig. 10: Schematic diagram of $z=300$ mm cross-section (a) and its acoustic pressure distribution at different tip shapes: (b) flat surface; (c) conical surface; (d) spherical surface

in Fig. 11. The acoustic pressure amplitudes along the AA₁ in the three cases are 1.171 MPa, 1.313 MPa, and 1.454 MPa, respectively. Higher acoustic pressure is obtained under the spherical rod compared to the other two tip shapes. The acoustic pressure distribution along BB₁ shows the same law. It can be seen that higher acoustic pressure gradients in the longitudinal and transversal directions can be induced in the case of the spherical rod, compared to the flat rod and the conical rod. In other words, a higher acoustic energy density is obtained within the melt under the spherical rods, corresponding to the excitation of a larger potential cavitation area.

The radiation of ultrasonic waves from the ultrasonic rod to the melt is essentially the propagation of ultrasonic waves at the solid-liquid interface. Theoretically, a flat radiating surface allows for vertical incidence and transmission of acoustic waves, resulting in higher utilization of acoustic energy^[34]. Over the years, the design of ultrasonic rods has been based on the design theory of ultrasonic amplitude transformers. Therefore, in many fields of ultrasonic processing, the ultrasonic rods are seen, whether exponential, stepped, or composite, to have a flat radiating surface. However, the actual situation is much more complicated for ultrasonic casting, especially for preparing large-size ingots. Although the acoustic energy utilization is high in the case of flat rods, the acoustic radiation range is small. The attenuation of the acoustic waves transmitted vertically into the metal melt is also intensified, therefore, the actual potential cavitation area is smaller than the conical rod and the spherical rod.

3.5 Effect of input pressure on acoustic field distribution

The effect of the input acoustic pressure on the acoustic field distribution of dual-frequency ultrasonic was investigated. The two ultrasonic frequencies are 15 kHz and 20 kHz, respectively, with equal input acoustic pressure. The rod spacing, angle, and insertion depth were set to 60 mm, 60°, and 30 mm, respectively. Figure 12 shows the acoustic pressure distribution and the corresponding cavitation area under different input acoustic pressures. The same pattern of acoustic pressure distribution is obtained since the conditions except total acoustic pressure were the same. The high acoustic pressure area in the melt is concentrated at the radiating surface of the ultrasonic rods and decays rapidly with the propagation of ultrasound. The closer to the radiating surface of the ultrasonic rods, the larger the acoustic pressure gradient is, which means the more serious the attenuation of acoustic pressure. As the propagation distance increases, the acoustic pressure attenuation tends to slow down, and the acoustic pressure shows a small increase at the bottom of the melt caused by the reflection from the inner wall of the crucible. The cavitation area is significantly affected by the input acoustic pressure. At low input pressure, only a minimal cavitation area is generated at the radiating surface of the ultrasonic rods, as shown in Figs. 12(a-c). As the input pressure increases, the effective cavitation region tends to expand gradually and extend from the radiating surface of the ultrasonic rods toward the core of the melt.

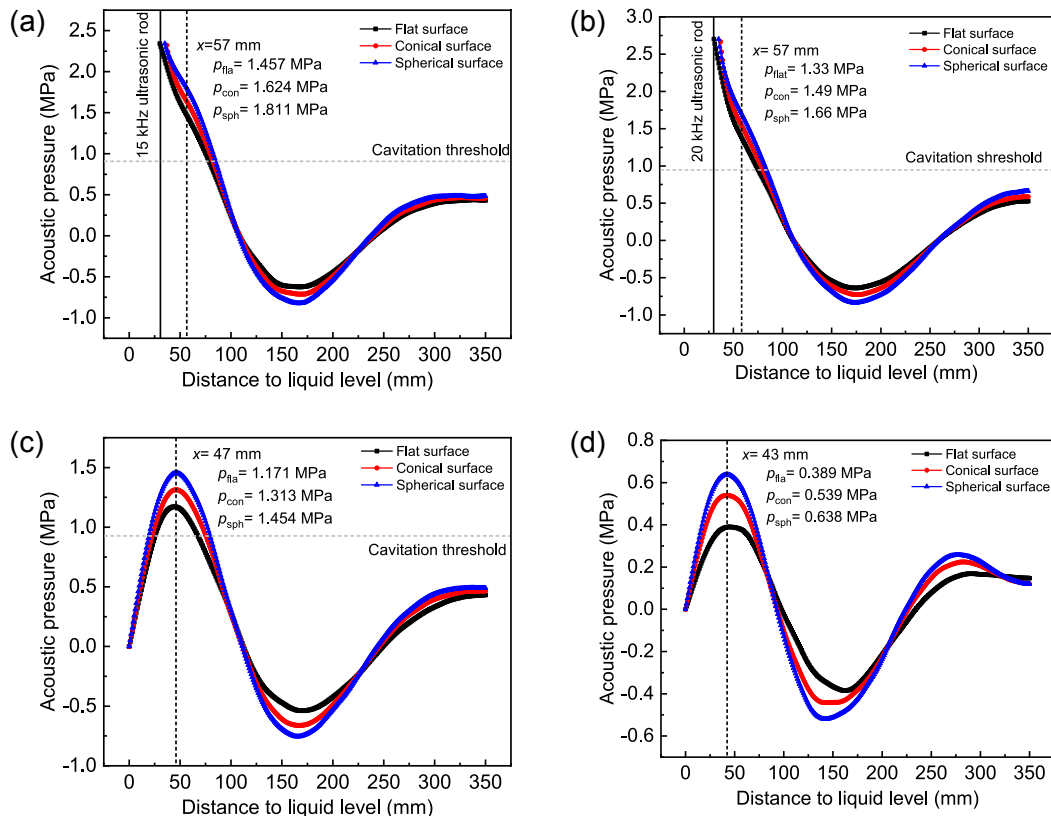


Fig. 11: Acoustic pressure distribution of dual-frequency ultrasonic treatment along Lines MM₁ (a), NN₁ (b), AA₁ (c), and BB₁ (d)

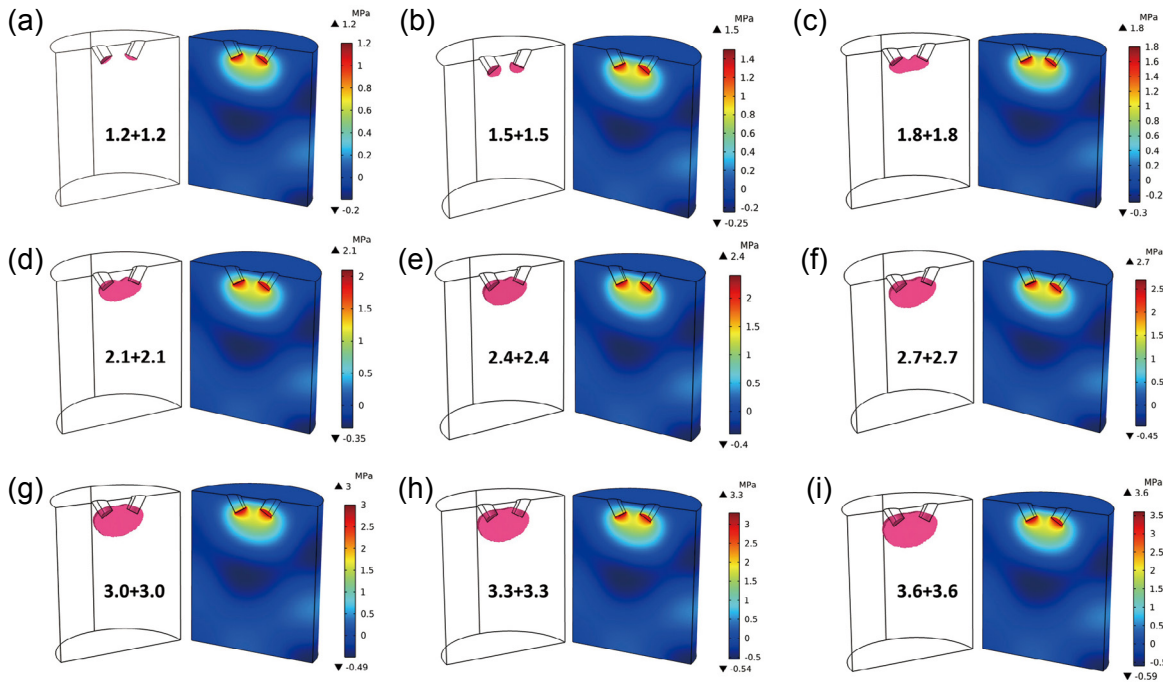


Fig. 12: Acoustic pressure distribution and corresponding cavitation area of dual-frequency ultrasonic treatment with different input pressures: (a) 1.2 MPa; (b) 1.5 MPa; (c) 1.8 MPa; (d) 2.1 MPa; (e) 2.4 MPa; (f) 2.7 MPa; (g) 3.0 MPa; (h) 3.3 MPa; (i) 3.6 MPa

To quantify the impact of input acoustic pressure on the cavitation effect, an integral calculation was conducted to determine the potential size of the cavitation region for different input acoustic pressures ranging from 1.2 MPa to 5.0 MP, as shown in Fig. 13. At low input acoustic pressure, the acoustic pressure rapidly decreases below the cavitation threshold due to the viscosity of the melt. As a result, only a small cavitation area is formed around the ultrasonic rods. For example, the effective cavitation volume is only $5.1 \times 10^3 \text{ mm}^3$ at an input acoustic pressure of 1.2 MPa. The potential cavitation volume increases linearly with the increase of the input acoustic pressure, and the cavitation volume expands to $8.7 \times 10^5 \text{ mm}^3$ with the further increase of input acoustic pressure to 5.0 MPa. The cavitation volume directly affects the efficiency of ultrasonic melt treatment. A more significant potential cavitation volume implies a more intense cavitation behavior, i.e., a more significant ultrasonic treatment effect. According to the numerical simulation results, increasing the initial input acoustic pressure as much as possible is an essential guarantee of obtaining a favorable ultrasonic treatment effect. However, it has been reported that the refinement effect of ultrasonication tends to weaken when the input pressure is increased to a certain level^[35]. The phenomenon can be attributed to the thermal effect of ultrasound resulting from excessive input acoustic pressure, which leads to a reduction in grain refinement efficiency. In addition, cavitation shielding also severely limits the cavitation effect, which is not concerned in this work. When the sound waves are launched into the liquid, numerous cavitation bubbles are created and gathered near the radiating surface, scattering and absorbing acoustic waves, which leads to a localization of the acoustic energy. This phenomenon is called cavitation shielding^[36-37]. Increasing the input ultrasonic power cannot

effectively destroy the cavitation shielding, but rather promotes the absorption of acoustic energy by the bubble cluster, further reducing the cavitation efficiency. Therefore, in practical casting experiments, a good grain refinement effect can be harvested by appropriately increasing the ultrasonic power. However, at too high input powers, cavitation shielding can cause a reduction in grain refinement effect. When the input pressure exceeds a threshold, the cavitation effect starts to decrease, which is not reflected in the simulation. To solve this problem, Moholkar et al.^[38] attempted to control bubble growth and cavitation modes by applying a dual-frequency ultrasonic field. The simulation results show that the cavitation bubble can be generated far away from the sound source by adjusting the characteristic parameters of ultrasonic field, which can effectively overcome the cavitation shielding. In view of the computational cost, cavitation shielding was not given consideration in this model.

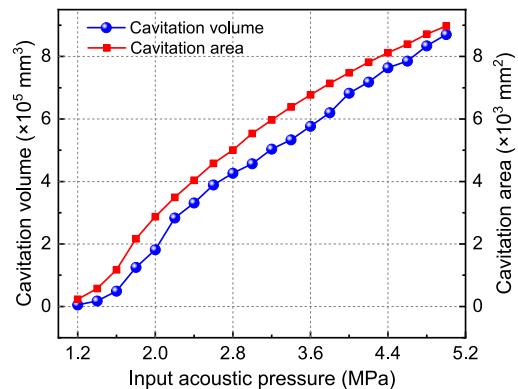


Fig. 13: Potential cavitation volume of dual-frequency ultrasonic treatment with different input acoustic pressures

3.6 Effect of acoustic pressure ratio on efficiency of ultrasonic

All the mentioned simulation studies were carried out based on the model with equal input acoustic pressure of the two ultrasound rods. The most crucial feature of dual-frequency ultrasonic is that two ultrasonic waves of different frequencies are introduced into the melt and produce a series of nonlinear acoustic effects, leading to a significant interaction-enhanced cavitation behavior. Therefore, the variation of the input pressure (p_0) ratio must significantly affect the effectiveness and efficiency of dual-frequency ultrasonic. In this subsection, a series of pressure ratios at 15 kHz and 20 kHz are defined to calculate the acoustic field distribution, with the same input p_0 of 2.7 MPa. The rod spacing, angle, and insertion depth were set to 60 mm, 60° , and 30 mm, respectively. Figure 14 illustrates the acoustic pressure distribution for pressure ratios from 10:1 to 1:10 ($P_{15}:P_{20}$). At high ratios, such as 10:1 and 1:10, a larger acoustic pressure region is formed only at the ultrasound rod with a higher pressure ratio, as shown in Figs. 14(a, b). Due to the extreme ratio, the higher p_0 ultrasound dominates the influence on the acoustic pressure distribution, leading to an imbalance in the acoustic pressure distribution, which is similar to the findings of previous studies on conventional

single-frequency ultrasonic treatment [24, 26]. With the shift of high ratio to equal ratio (1:1), the unbalanced acoustic pressure distribution gradually develops toward the axisymmetric distribution. When the pressure ratio is 1:1, the acoustic pressure distribution in the melt is almost entirely axisymmetric, as shown in Fig. 14(f). It is also noteworthy that as the high ratio shifts to the equal ratio, the acoustic pressure contour surface near the ultrasound rods shifts from dense to sparse, which indicates that the attenuation of the acoustic pressure is slowed down.

The effective cavitation range corresponds to the acoustic pressure distribution. Figure 15 illustrates the cavitation area for different pressure ratios. At high ratios, such as 10:1 and 1:10, the effective cavitation range tends to cluster near the radiating surface of the ultrasonic rod with a higher p_0 . As the ratio approaches equality, the cavitation volume gradually increases and the cavitation volume gradually increases. The distribution of the cavitation region gradually develops axisymmetrically and extends to the crucible center. Figure 16 exhibits the statistical results of the cavitation volume. The pressure ratio plays a crucial role in cavitation effect. At high ratios, only a tiny cavitation volume is obtained at the ultrasonic rod position. The cavitation volume gradually

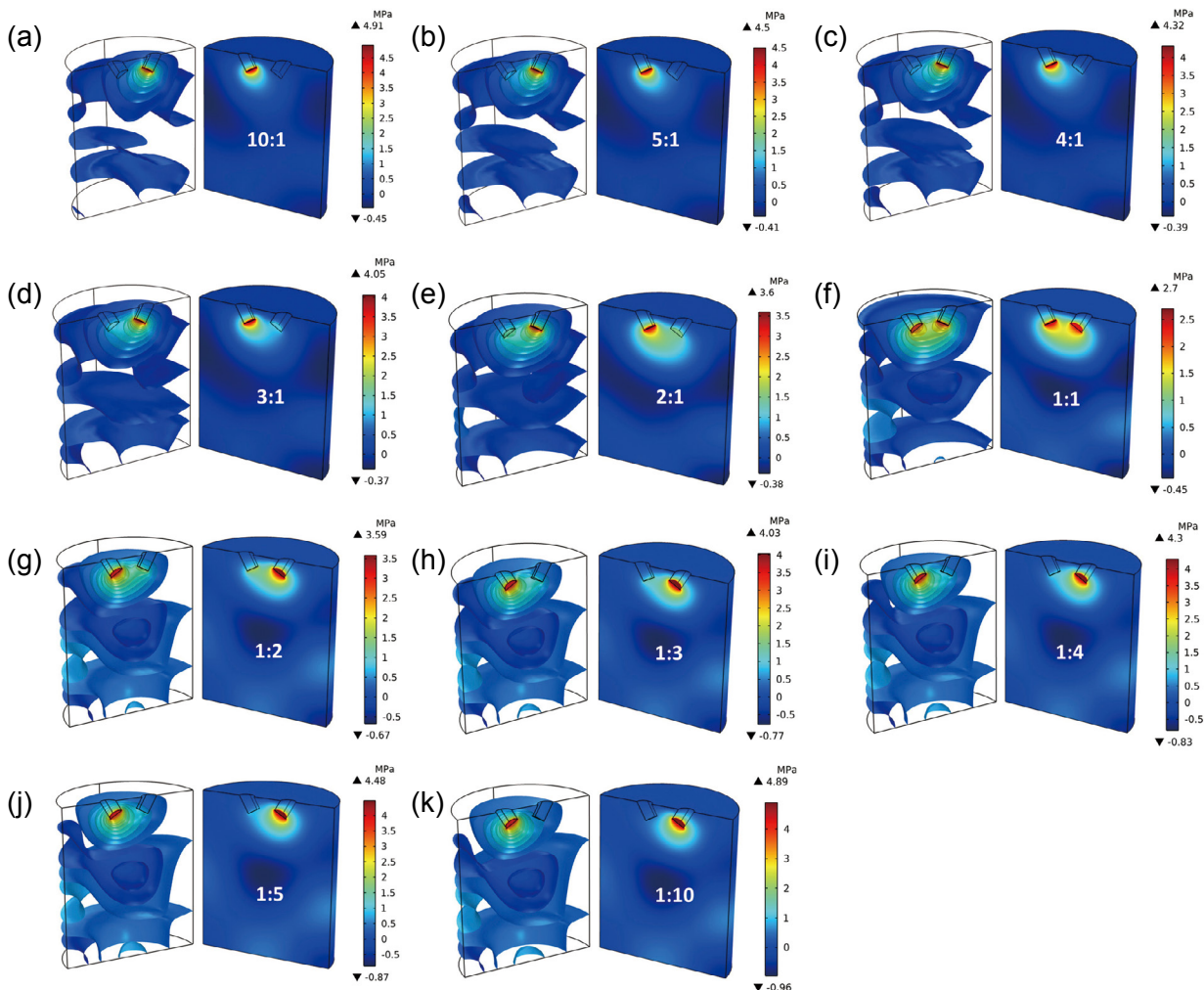


Fig. 14: Acoustic pressure distribution of dual-frequency ultrasonic treatment with different acoustic pressure ratios: (a) 10:1; (b) 5:1; (c) 4:1; (d) 3:1; (e) 2:1; (f) 1:1; (g) 1:2; (h) 1:3; (i) 1:4; (j) 1:5; (k) 1:10

increases as the ratio approaches equality. The results indicate an interactive enhancement between the two different frequencies of ultrasonic waves, which is significantly affected by the pressure ratio. The cavitation volume of the 15 kHz-dominated dual-frequency ultrasonic (from 10:1 to 2:1) is larger than that of the corresponding 20 kHz-dominated dual-frequency ultrasonic (from 1:10 to 1:2). It is noteworthy that the maximum cavitation volume is obtained at the ratio of 2:1, rather than 1:1.

An analysis of the acoustic pressure distribution along different sectional lines was carried out to gain a deeper understanding of the significant differences in the potential cavitation range at different ratios of dual-frequency ultrasonic. Figure 17(a) shows the acoustic pressure distribution along the central axis OO_1 . The acoustic pressure increases sharply from

the liquid level to the end of the ultrasonic radiating rods and then begins to decay. The maximum acoustic pressure amplitude is obtained in the case of the 2:1 ratio. A similar pattern was observed for the acoustic pressure distribution along PP_1 (a truncated line on the $Z=300$ mm cross-section, as shown in Fig. 1), as shown in Fig. 17(b). These results imply that the 2:1 ratio increases not only the axial but also radial acoustic pressure, which is closely related to the interaction of the two frequencies of ultrasonic waves during propagation in the melt. At high ratios, the acoustic pressure distribution dominated by ultrasonic waves of a specific frequency (15 kHz or 20 kHz) is extremely asymmetric, weakening the interaction between frequencies. The interaction between two frequencies of equal ratio is stronger compared to that of high ratios. The interactive enhancement can be further improved by appropriately increasing the ratio of the 15 kHz ultrasound. At a ratio of 2:1, this intense interactive enhancement leads to an increase in the average acoustic pressure within the melt and slows down the attenuation of acoustic pressure. As a result, it allows for achieving a larger potential cavitation area.

To improve the efficiency of dual-frequency ultrasonic treatment, it is necessary to choose the appropriate pressure ratio. The maximum cavitation area is obtained at a ratio of 2:1 for 15 kHz and 20 kHz ultrasound.

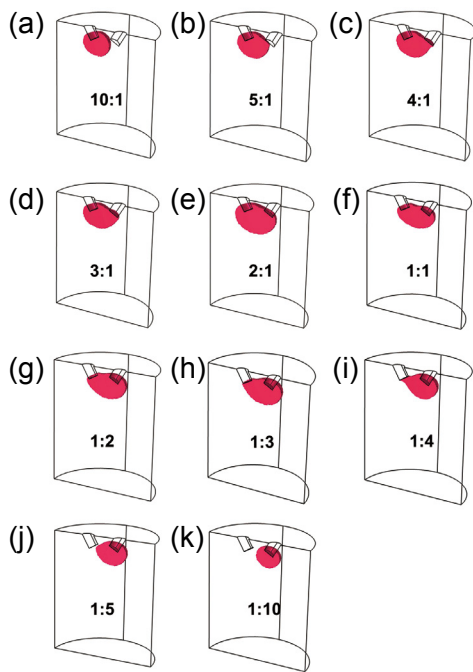


Fig. 15: Potential cavitation region of dual-frequency ultrasonic treatment with different pressure ratios: (a) 10:1; (b) 5:1; (c) 4:1; (d) 3:1; (e) 2:1; (f) 1:1; (g) 1:2; (h) 1:3; (i) 1:4; (j) 1:5; (k) 1:10

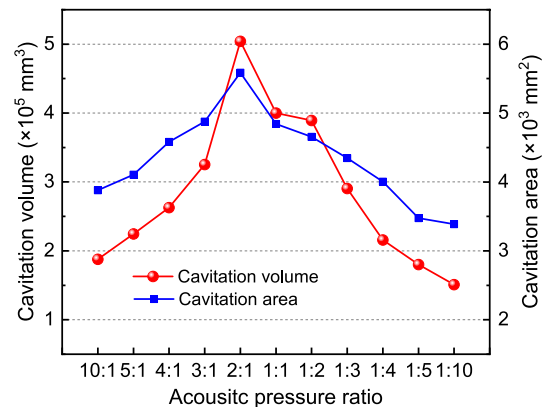


Fig. 16: Potential cavitation volume and area of dual-frequency ultrasonic treatment with different pressure ratios

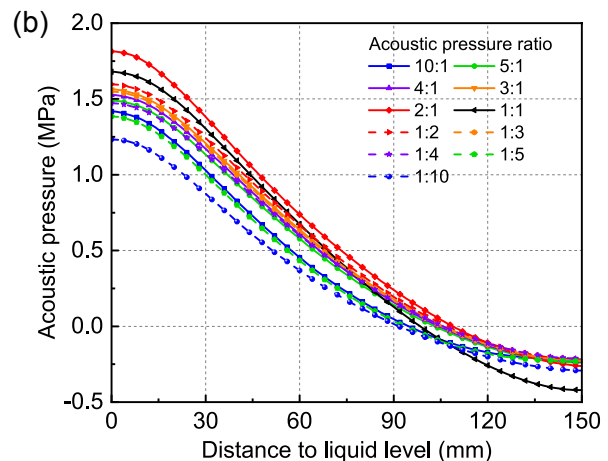
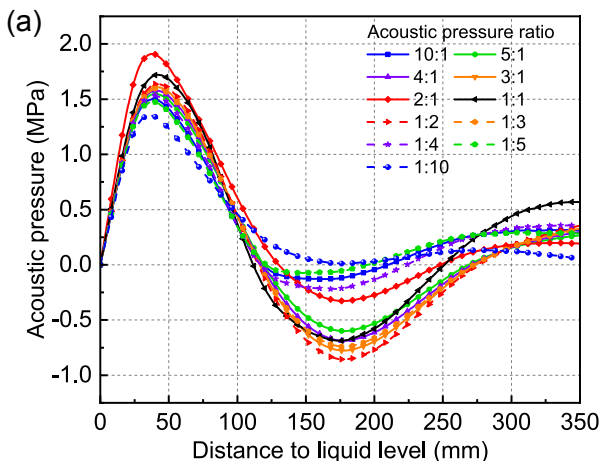


Fig. 17: Acoustic pressure distribution of dual-frequency ultrasonic treatment along OO_1 (a) and PP_1 (b)

4 Conclusions

In this work, a transient 3D model was established to investigate the effects of spatial interaction of two ultrasounds on the acoustic field of dual-frequency ultrasonic treatment. The effects of the spatial position and tip shape of the ultrasound rod, input pressures and their ratio on the acoustic pressure distribution and corresponding cavitation region were thoroughly analyzed. The experimental material used for these investigations was AZ80 alloy. By examining these factors in detail, a comprehensive understanding can be obtained as follows:

(1) The interaction of the two ultrasounds is weakened with the increase of the ultrasonic rod spacing, and the maximum cavitation volume is obtained at the rod spacing of 60 mm.

(2) At small included angles (from 0° to 60°), the cavitation region increases slightly. Further increasing the angle will reduce the cavitation volume obviously.

(3) As the insertion depth increases, the attenuation degree of acoustic pressure below the ultrasonic rod increases at first and then decreases. The maximum cavitation volume is obtained at the insertion depth of 50 mm.

(4) The spherical rod mitigates the longitudinal and transversal attenuation of acoustic pressure. The cavitation volume of the spherical rod is 53.7% and 31.7% larger than the flat and conical rods, respectively.

(5) The increasing input pressure will enlarge the cavitation region, but will not affect the acoustic pressure distribution pattern. The pressure ratio significantly affects the acoustic pressure distribution, and the optimal cavitation effect is obtained at a ratio of 2:1.

Acknowledgments

This work was financially supported by the National Natural Science Foundation of China (Grant Nos. 51974082 and 52274377), the Fundamental Research Funds for the Central Universities (Grant No. N2209001), and the Programme of Introducing Talents of Discipline Innovation to Universities 2.0 (the 111 Project 2.0 of China, Grant No. BP0719037).

Conflict of interest

The authors declare that they have no known competing financial interests or personal relationships that could have appeared to influence the work reported in this paper.

References

- [1] Arefi-Oskoui S, Khataee A, Safarpour M, et al. A review on the applications of ultrasonic technology in membrane bioreactors. *Ultrasonics Sonochemistry*, 2019, 58: 104633. <https://doi.org/10.1016/j.ultsonch.2019.104633>.
- [2] Jia Z, Yu B, Lan Q, et al. Effect of ultrasonic field treatment on degassing of 2024 alloy. *China Foundry*, 2021, 18(2): 124–130.
- [3] Eskin G I. Broad prospects for commercial application of the ultrasonic (cavitation) melt treatment of light alloys. *Ultrasonics Sonochemistry*, 2001, 8: 319–325.
- [4] Bjorno L. Forty years of nonlinear ultrasound. *Ultrasonics*, 2002, 40: 11–17. [https://doi.org/10.1016/S0041-624X\(02\)00084-7](https://doi.org/10.1016/S0041-624X(02)00084-7).
- [5] Eskin D G, Tzanakis I, Wang F, et al. Fundamental studies of ultrasonic melt processing. *Ultrasonics Sonochemistry*, 2019, 52: 455–467. <https://doi.org/10.1016/j.ultsonch.2018.12.028>.
- [6] Cui Y, Xu C L, Han Q Y. Microstructure improvement in weld metal using ultrasonic vibrations. *Advanced Engineering Materials*, 2007, 9(3): 161–163. <https://doi.org/10.1002/adem.200600228>.
- [7] Han Z H, Wang Z M, Sun Z P, et al. Influence of non-uniform ultrasonic vibration on casting fluidity of liquid aluminum alloy. *China Foundry*, 2022, 19(5): 380–386. <https://doi.org/10.1007/s41230-022-2039>.
- [8] Liu Y X, Han Q Y, Li H, et al. Numerical and experimental investigation of upsetting with ultrasonic vibration of pure copper cone tip. *Ultrasonics*, 2013, 53(3): 803–807. <https://doi.org/10.1016/j.ultras.2012.11.010>.
- [9] Eskin G I. *Ultrasonic treatment of light alloy melts*. CRC Press, 1997.
- [10] Eskin G I. Cavitation mechanism of ultrasonic melt degassing. *Ultrasonics Sonochemistry*, 1995, 2(2): S137–S141. [https://doi.org/10.1016/1350-4177\(95\)00020-7](https://doi.org/10.1016/1350-4177(95)00020-7).
- [11] Ansyutina A E, Gur'ev I I, Eskin G I, et al. Ultrasonic treatment of alloy MA2-1 during solidification. *Metal Science and Heat Treatment*, 1972, 14(8): 677–679. <https://doi.org/10.1007/BF00647907>.
- [12] Alba-Baena N, Pabel T, Villa-Sierra N, et al. Effect of ultrasonic melt treatment on degassing and structure of aluminium alloys. *Materials Science Forum*, 2013, 765: 271–275. <https://doi.org/10.4028/www.scientific.net/MSF.765.271>.
- [13] Wu W H, Zhai W, Wang J Y, et al. Progress of cavitation and acoustic streaming dynamics of liquid materials within ultrasonic field. *Scientia Sinica Technologica*, 2022, 52: 2–27. <https://doi.org/10.1360/SST-2022-0018>.
- [14] Childs W J, Frawley J J. Dynamic nucleation of supercooled metals. *Transactions of the Metallurgical Society of AIME*, 1968, 242(2): 629–634.
- [15] Wang S, Kang J W, Guo Z P, et al. In situ high speed imaging study and modelling of the fatigue fragmentation of dendritic structures in ultrasonic fields. *Acta Materialia*, 2018, 165: 388–397. <https://doi.org/10.1016/j.actamat.2018.11.053>.
- [16] Xu Z W, Li Z W, Zhong S J, et al. Wetting mechanism of Sn to Zr50.7Cu28Ni9Al12.3 bulk metallic glass assisted by ultrasonic treatment. *Ultrasonics Sonochemistry*, 2018, 48(1): 207–217. <https://doi.org/10.1016/j.ultsonch.2018.05.036>.
- [17] Zhao J T, Wu X Y, Ning L P, et al. Wetting of aluminium and carbon interface during preparation of Al-Ti-C grain refiner under ultrasonic field. *Ultrasonics Sonochemistry*, 2021, 76(1–2): 105633. <https://doi.org/10.1016/j.ultsonch.2021.105633>.
- [18] Swamy K M, Narayana K L. Intensification of leaching process by dual-frequency ultrasound. *Ultrasonics Sonochemistry*, 2001, 8(4): 341–346. [https://doi.org/10.1016/S1350-4177\(01\)00067-0](https://doi.org/10.1016/S1350-4177(01)00067-0).
- [19] Ning S C, Chen X R, Le Q C, et al. Effect of ultrasonic frequency on cavitation behavior, microstructure and mechanical properties of AZ80 magnesium alloy. *Materials Research Express*, 2019, 6(8): 0865d9. <https://doi.org/10.1088/2053-1591/ab24f0>.
- [20] Feng R, Zhao Y Y, Zhu C P, et al. Enhancement of ultrasonic cavitation yield by multi-frequency sonication. *Ultrasonics Sonochemistry*, 2002, 9: 231–236. [https://doi.org/10.1016/S1350-4177\(02\)00083-4](https://doi.org/10.1016/S1350-4177(02)00083-4).
- [21] Brotchie A, Grieser F, Ashokkumar M. Sonochemistry and sonoluminescence under dual-frequency ultrasound irradiation in the presence of water-soluble solutes. *The Journal of Physical Chemistry: C*, 2008, 112(27): 10247–10250. <https://doi.org/10.1021/jp801763v>.

- [22] Qin L M, Yang X A, Leng D, et al. Dual-frequency ultrasound assisted-enzyme digestion coupled with atomic fluorescence spectrometry as a green and efficient tool for cadmium detection in rice flour samples. *Talanta*, 2018, 188: 308–315. <https://doi.org/10.1016/j.talanta.2018.06.007>.
- [23] Chen X R, Ning F K, Hou J, et al. Dual-frequency ultrasonic treatment on microstructure and mechanical properties of ZK60 magnesium alloy. *Ultrasonics Sonochemistry*, 2018, 40(Pt A): 433–441. <https://doi.org/10.1016/j.ultsonch.2017.07.027>.
- [24] Yin Z Y, Le Q C, Chen X R, et al. The grain refinement of Mg alloy subjected to dual-frequency ultrasonic melt treatment: A physical and numerical simulation. *Journal of Materials Research and Technology*, 2022, 21: 1554–1569. <https://doi.org/10.1016/j.jmrt.2022.10.016>.
- [25] Sáez V, Frías-Ferrer A, Iniesta J, et al. Characterization of a 20 kHz sonoreactor. Part I: Analysis of mechanical effects by classical and numerical methods. *Ultrasonics Sonochemistry*, 2005, 12(1–2): 59–65. <https://doi.org/10.1016/j.ultsonch.2004.06.011>.
- [26] Chen X R, Jia Y H, Le Q C, et al. Understanding dual-frequency ultrasonic melt treatment on grain refinement and mechanical properties improvement of AZ80 magnesium alloy: experiment and simulation. *Journal of Materials Research and Technology*, 2021, 15: 4758–4767. <https://doi.org/10.1016/j.jmrt.2021.10.083>.
- [27] Cao P L, Hao C C, Ma C, et al. Physical field simulation of the ultrasonic radiation method: An investigation of the vessel, probe position and power. *Ultrasonics Sonochemistry*, 2021, 76: 105626. <https://doi.org/10.1016/j.ultsonch.2021.105626>.
- [28] Sreekumar V M, Babu N H, Eskin D G. Potential of an Al-Ti-MgAl₂O₄ master alloy and ultrasonic cavitation in the grain refinement of a cast aluminum alloy. *Metallurgical and Materials Transactions: B*, 2017, 48(1): 208–219. <https://doi.org/10.1007/s11663-016-0824-5>.
- [29] Eskin D G, Tzanakis I, Wang F, et al. Fundamental studies of ultrasonic melt processing. *Ultrasonics Sonochemistry*, 2019, 52: 455–467. <https://doi.org/10.1016/j.ultsonch.2018.12.028>.
- [30] Ye L Z, Zhu X J, Liu Y. Numerical study on dual-frequency ultrasonic enhancing cavitation effect based on bubble dynamic evolution. *Ultrasonics Sonochemistry*, 2019, 59: 104744. <https://doi.org/10.1016/j.ultsonch.2019.104744>.
- [31] Wang X J, Ning Z, Lv M, et al. The enhanced effect of collapse strength of a dual-frequency driven bubble in 2-dimensional space. *Results in Physics*, 2021, 29: 104727. <https://doi.org/10.1016/j.rinp.2021.104727>.
- [32] Eskin D G. Ultrasonic melt processing: Achievements and challenges. *Materials Science Forum*, 2015, 828–829: 112–118. <https://doi.org/10.4028/www.scientific.net/MSF.828-829.112>.
- [33] Chen X R. Study on solidification behavior of magnesium alloy melt by variable-frequency/dual-frequency ultrasonic treatment. Master dissertation, Northeastern University, 2018. <https://doi.org/10.27007/d.cnki.gdbeu.2018.001075>.
- [34] Guo D Z, Li X Q, Chen D X, et al. Effects of tip-shape of ultrasonic radiator on microstructure of aluminium alloy. *Special Casting & Nonferrous Alloys*, 2011, 31(10): 969–973. <https://doi.org/10.3870/tzzz.2011.10.025>. (In Chinese)
- [35] Hu Y Q, Jiang R P, Li X Q. Comparative study on the effect of ultrasonic power on the microstructure and mechanical properties of 2195 aluminum alloy ingot. *Frontiers in Materials*, 2022, 9: 827476. <https://doi.org/10.3389/fmats.2022.827476>.
- [36] Ying C F, Bai L X, Li C, et al. Cavitation field from a horn – A new model. *Science China: Physics, Mechanics and Astronomy*, 2011, 54(1): 74–78. <https://doi.org/cnki:sun:jgxxg.0.2011-01-010>.
- [37] Pishchalnikov Y A, Mcateer J A, Bailey M R, et al. Acoustic shielding by cavitation bubbles in shock wave lithotripsy (SWL). *American Institute of Physics*, 2006, 319–322. <https://doi.org/10.1063/1.2210369>.
- [38] Moholkar V S, Rekveld S, Warmoeskerken M M C G. Modeling of the acoustic pressure fields and the distribution of the cavitation phenomena in a dual frequency sonic processor. *Ultrasonics*, 2000, 38(1): 666–670. [https://doi.org/10.1016/S0041-624X\(99\)00204-8](https://doi.org/10.1016/S0041-624X(99)00204-8).